Received December 23, 2019, accepted December 27, 2019, date of publication December 31, 2019,
date of current version January 8, 2020.

Digital Object Identifier 10.1109/ACCESS.2019.2963284

Single-Phase Grid-Tied Transformerless Inverter of Zero Leakage Current for PV System

AHMAD H. SABRY[1], ZEINA MUEEN MOHAMMED[2], FARAH HANI NORDIN[1], N. H. NIK ALI[1], AND ALI SAADON AL-OGAILI[1]

[1]Institute of Power Engineering, Universiti Tenaga Nasional (UNITEN), Kajang 43000, Malaysia
[2]Division of Government Contracts, Baghdad University, Baghdad 10071, Iraq

Corresponding author: Ahmad H. Sabry (ahs4771384@gmail.com)

This work was supported by the Universiti Tenaga Nasional (UNITEN) for the UNIIG fund (Project Code: J510050802) given to support this project.

ABSTRACT Multi-level transformerless inverters are widely used in grid-tied PV systems since they characterized by higher efficiency and lower cost. In this context, new topologies, modulation, and control schemes were presented to solve problems of a common-mode voltage and leakage current. This work proposes a transformerless five-level inverter with zero leakage current and ability to reduce the harmonic output content for a grid-tied single-phase PV system. The neutral of the grid links to a common on which the negative and the positive terminals of the DC-link are connected via parasitic capacitors that can eliminate the leakage current. The proposed topology, with its inherent circuit structure, leads to boost the overall efficiency. Simulation and experimental results show almost zero leakage current and a high-quality output when maintaining balanced capacitor voltages on the DC-link input. The experimental results show 1.07% THD and 96.3 % maximum efficiency when injecting a power of 1.1 kW that verify the performance of the proposed inverter with PV sources.

INDEX TERMS IGBT inverters, transformerless grid-connected photovoltaic inverter, solar PV.

NOMENCLATURE

5L-NPC	5-level neutral point clamped converter
Δv	The maximum allowable ripple of the voltage
K_{PV}	The utilization ratio of the average power generated by PV divided by its power at MPP.
P_{MPP}	Power at the maximum power point
α	Taylor approximation coefficient = -0.0161
V_{MPP}	The voltage at the maximum power point
β	Taylor approximation coefficient = 1.0276
P_{PV}	Photovoltaic power
V_{PV}	PV voltage
i_{PV}	PV current
γ	Taylor approximation coefficient = -11.7038
v_{cm}	Common-mode voltage
v_{1N}	The voltage of terminal 1 w.r.t the neutral (N)
v_{2N}	The voltage of terminal 2 w.r.t the neutral (N)
v_{cm-dm}	Common-mode voltage in Fig. 3
L_2	Inductance value in Fig. 3
L_1	Inductance value in Fig. 3
$\frac{dv_{c_k}}{dt}$	voltage rate of change across the DC capacitors
i_{c_k}	Capacitor current
c_k	Capacitor k $\in$ 1, 4}
S_k	Switch state = 0 for OFF state and = 1 for ON
V_{dc}	DC-link voltage
d_{init}	Initial value for v_{dc_ref}.
v_{dc_ref}	Reference voltage DC value
d_{max}, d_{min}	Upper and lower limit for v_{dc_ref}.
Δd	Increment value for increase/decrease v_{dc_ref}.
V_{CE}	IGBT collector-emitter voltage drop at load
V_t	IGBT voltage drops at no load
V_{AK}	Diode anode-cathode voltage drop at load
V_f	Diode anode-cathode voltage drop at no load
R_{CE}	IGBT ON-state resistances
R_d	Diode ON-state resistances
$i\,(t)$	Output current
i_o	The amplitude of the output current
P_{onIGBT}	The power loss of IGBT on-state
m	Modulation index
$P_{onDiode}$	The power loss of diode on-state
$P_{offIGBT}$	The power loss of IGBT off-state
$P_{offDiode}$	The power loss of diode off-state
MPPT	Maximum power point tracking

The associate editor coordinating the review of this manuscript and approving it for publication was Tariq Masood.

I. INTRODUCTION

Photovoltaic (PV) power as renewable energy is more and more popular recently, but the power fluctuations harm the quality and stabilization of the grid voltage and frequency. Several articles have published recently with different control strategies for grid integrated PV systems such as a modified sine-cosine optimized (MSCO) [1], fuzzy space vector PWM [2], and intelligent fuzzy [3], these algorithms merged with the particle swarm optimization (PSO) to get maximum power extraction from a PV with a high convergence velocity. An adaptive neuro-fuzzy inference system with a PSO and maximum power point tracker (MPPT) method discussed to improve the PV power and oscillation tracking using a space vector modulation hysteresis current controller in [4]. A controller's design for optimal hybrid renewable power using Lyapunov function without MPPT offered by [5] and Jaya-based MPPT in [6]. Although all these recent findings achieved a good power extraction with fast MPPT, the inverter topology, design, grid leakage current were not discussed.

A common solution recommends two types of transformerless inverter in the literature in this concern, 1) Single-Stage Power Conversion and 2) Multi-Stage Power Conversion. In both cases, the inverters are the most critical part of PV systems, as they play the main role in the stability of large-scale PV systems [7]. To enhance the system reliability and life span, Multi-level inverters (MLIs), for high voltage and power applications, are growing day by day, especially when being integrated into grid-tied PV systems. One of the effective topologies of MLIs is the 5-level neutral point clamped converter (5L-NPC). Several MLI topologies were proposed in the literature that can be classified as in Fig. 1.

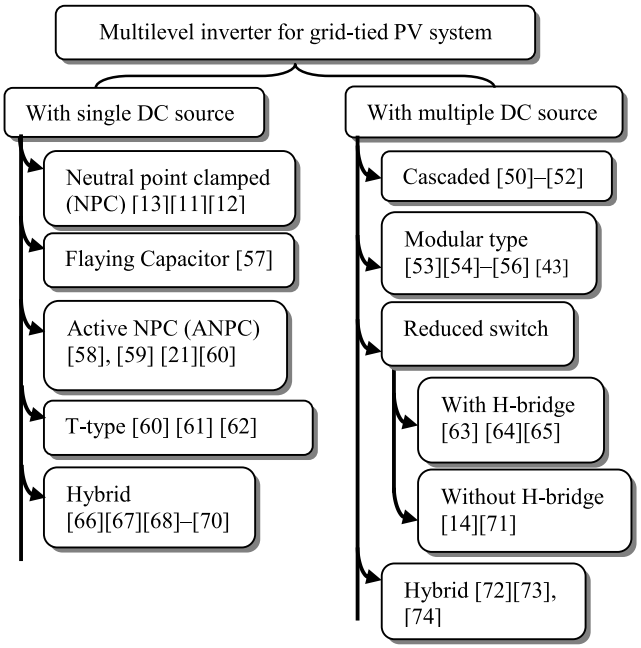

FIGURE 1. Common MLI topologies.

The conventional two-level inverters in grid-tied PV systems were found inappropriate for medium and high voltage utility grid [8], [9] due to high harmonics in the injected grid current [10]. In contrast, MLIs are more appropriate for medium and high voltage utility grid to interface with PV systems [10]. MLIs present a higher quality output voltage with lower total harmonic distortion (THD), lower $^{dv}/_{dt}$ switches stress, less need for passive filter components [11]–[13]. In PV grid-tied inverter systems, high-frequency common-mode (CM) voltages need to be avoided due to its causes of the charging/discharging current to flow through the inverter to ground. This leakage current will lead to an increase in losses, current harmonics, safety issues, and interference problems of electromagnetic effects [14]–[18]. For grid-tied PV residential systems, energy generation and the time required to pay back are highly depending on the inverter's efficiency and reliability. Therefore, they are considered as the most important features for PV inverter systems. Although five-level inverters have interesting characteristics enabling them to operate in transformerless PV systems, two main limitations should be considered in designing; 1) the balancing issue of the DC-link capacitors' voltages that required for a proper operation [19], and 2) the conduction power losses, especially when the inverter operates with reactive power to achieve a bidirectional path through a freewheeling state.

This work develops a system that includes a 5L-NPC inverter with a control strategy maintaining the desired voltages balancing for the input DC-link of a transformerless grid-tied single-phase PV system. It allows zero leakage current and the ability to reduce the harmonic content of the output. The neutral of the grid links to a common on which the negative and positive terminals of the DC-link are connected via parasitic capacitors that can eliminate the leakage current. It is not possible to solve the unbalancing problem of the DC-link capacitor voltage in single-phase NPC converters using one of the three-phase techniques like adding zero-sequence voltage [20]. This work solves the unbalancing problem by developing a modulation strategy [21] that controlling the DC-link capacitor voltages to follow a required reference value and creates the required AC output voltage despite the dynamic capacitor voltage values.

A. PV MODULE REQUIREMENTS

The solar PV module/cell is very sensitive to the ripples of output current that affect the available power significantly but do not damage the PV cell. The inverter in PV powered residential systems must be controlled by one of the MPPT technologies to capture the maximum yield PV energy. Basing on the analysis of the circuit shown in Fig. 2, it is essential to decrease the excessive variation and ripple at the PV output. The maximum allowable ripple of the voltage (Δv) has been defined in [22], [23] as:

$$\Delta v = \sqrt{\frac{2\,(K_{PV}-1)\,P_{MPP}}{3\alpha V_{MPP}+\beta}} = 2\sqrt{\frac{(K_{PV}-1)\,P_{MPP}}{d^2_{P_{PV}}/dV^2_{PV}}} \qquad (1)$$

where P_{MPP}, and V_{MPP} denote MPP power, and voltage respectively. K_{PV} is the utilization ratio of the average power

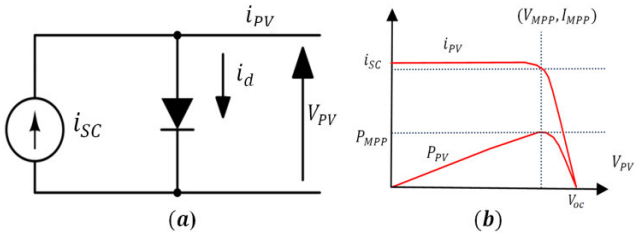

FIGURE 2. Characteristics and model of a PV cell: (a) electrical model with current and voltage defined and (b) electrical characteristics of PV cell.

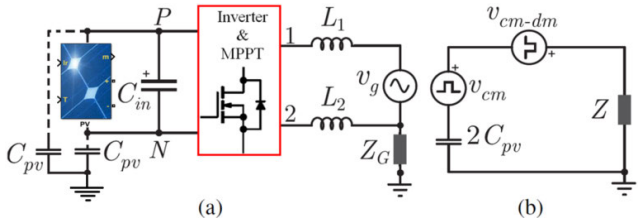

FIGURE 3. Equivalent circuit of a common-mode single-phase transformerless topology [16]. (a) Inverter topology. (b) Common-mode scheme.

generated by PV divided by its power at MPP. β, γ, and α denote the coefficients of Taylor approximation of a PV current. These coefficients can be given by [22]:

$$i_{PV} = \alpha V_{PV}^2 + \beta V_{PV} + \gamma \tag{2}$$

$$V_{PV} \approx V_{MPP} + \Delta v \sin(\omega t) \tag{3}$$

$$\alpha = \frac{1}{2}\frac{d^2 I_{MPP}}{dV^2{}_{MPP}} \tag{4}$$

$$\beta = \frac{dI_{MPP}}{dV_{MPP}} - 2\alpha V_{MPP} \tag{5}$$

$$\gamma = \alpha V_{MPP}^2 - \frac{dI_{MPP}}{dV_{MPP}} V_{MPP} + I_{MPP} \tag{6}$$

In order to keep a low estimated error of a PV power, the utilization ratio must not exceed the value of 0.98%. For example, for BP4160, 160 W, monocrystalline PV module, the parameters can be calculated according to the equations (1-6) as; $\alpha = -0.0161$, $\beta = 1.0276$, and $\gamma = -11.7038$. Therefore, the maximum allowable ripple of the voltage (Δv) is less than 8.5% of the voltage at MPP. Furthermore, for a PV module with an MPP voltage of 35V, the 98% utilization ratio allows a ripple voltage amplitude not higher than 3V.

B. LEAKAGE CURRENT AND PARASITIC CAPACITANCE ISSUES

Although using a transformer will remove the effects of parasitic capacitance and leakage current for grid-tied PV systems, it confirms the galvanic isolation between the grid and PV modules. In contrast, for systems with a transformerless inverter, the link between the PV modules and the grid creates a galvanic connection, which can produce a CM resonant circuit [16], [24]. One solution can electrify the issue of the resonant circuit but may produce higher leakage current to ground that depends on the control scheme and topology structure [16], [25]. For a generalized transformerless inverter with full-bridge topology for a single-phase grid-connected PV residential system, a CM equivalent circuit [16] can be shown in Fig. 3.

According to [16], v_{cm} and v_{cm-dm} are given by:

$$v_{cm} = \frac{v_{1N} + v_{2N}}{2}$$

$$v_{cm-dm} = (v_{1N} + v_{2N})\frac{(L_2 - L_1)}{2(L_2 + L_1)} \tag{7}$$

In general, four modulation strategies are used to control the switches of an inverter, bipolar, unipolar, discontinuous, and hybrid modulation [26]. A single-phase full-bridge inverter (H4) is a well-known and basic topology for PV applications, in which the common-mode voltage can be clamped to DC-link voltage (V_{DC}) and to zero for the rest of the period. As a result, the common mode frequency is similar to the grid frequency that leads to reduce the leakage current due to the absence of high-frequency components. The limitations of H4 is the current ripples that can be reduced by either adding bulky inductors or using a higher switching frequency, but both of them causes lower system efficiency. H5 topology [27] has reduced this by adding an extra switch to the full-bridge of H4.

Several studies addressed approaches to reduce the leakage current in which freewheeling pathways were produced to decouple the grid from solar PV modules at null states of the DC side H5 [27] or AC side [28], and H6 [29] [30], [31]. Those systems offer a straightforward structure scheme, but their common-mode voltages are affected by the leakage current loop via its parasitic parameters that can bring an ineffective reduction of leakage currents [32], [33]. Inverter with common-ground is a topology that increasingly interested in mitigating the leakage currents [34], [35]–[39]. The common-mode voltage becomes zero when connecting the neutral-line of a grid directly to a PV negative terminal [40]. The topology of common-ground of a virtual DC-bus has presented in [35] in which a virtual DC-bus is created via a capacitor that provides a negative output voltage which is varied in some operation modes. A concept of charge pump topology was offered in [36], in which the two stages of the charge transfer process increase in topology components such as the power switching devices. A significant interest with the common-ground inverter has proposed in [41], which offers a reduction switch-count of a PWM-based unipolar circuit. An inverter of a common-ground multilevel transformerless type was presented in [42] that releases of a switched capacitor, this topology offers a reduction in the number of switches and needs a large number of input voltages over the Full-Bridge (FB) based circuits.

The contributions in this work are; 1) Converging the leakage current to zero by connecting the DC-link of the PV to stray capacitors into a common with the gird neutral terminal to reduce the harmonic content in the

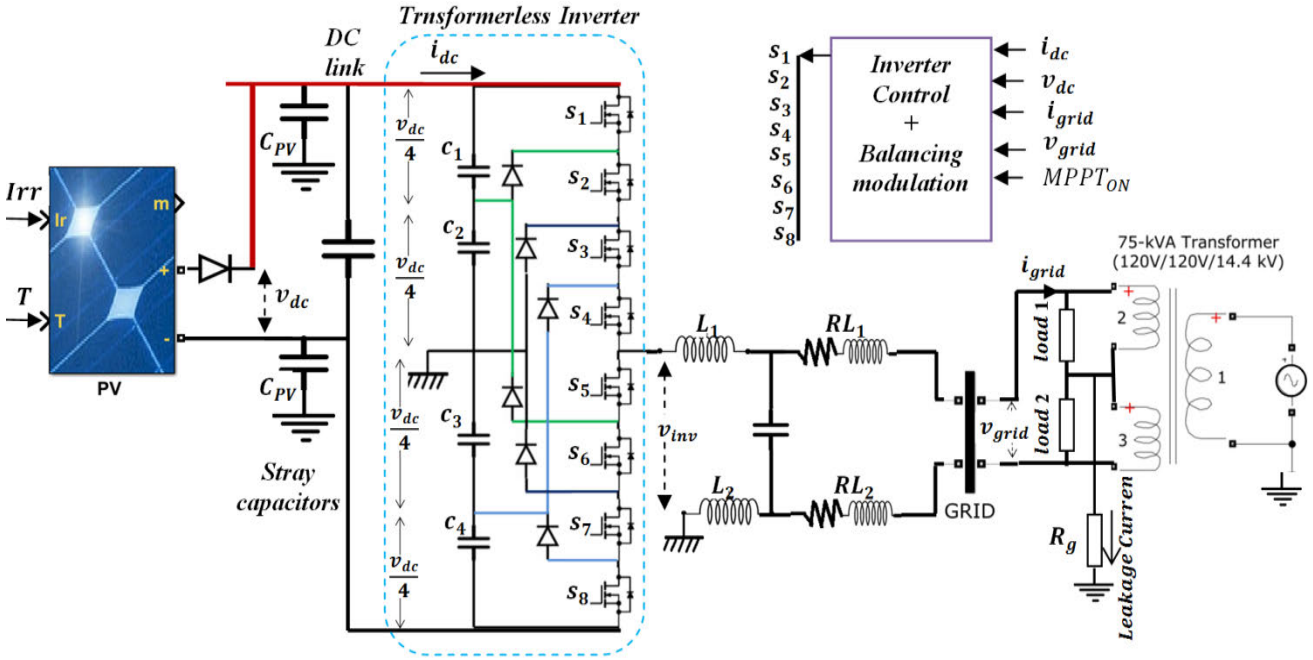

FIGURE 4. Proposed Single-Phase Grid-tied with 5L-NPC transformerless inverter topology.

5L-NPC inverter. 2) Solving unbalancing problems of this topology by developing a modulation control strategy, inspired by [21], that controlling the DC-link capacitor voltages to follow a required reference value, and to create the required AC output voltage despite the dynamic capacitor voltage values. 3) Employing a transformerless 5L-NPC controlled by MPPT method with Perturb and Observe (P&O) algorithm in a solar PV grid-tied single-phase system. Therefore, the function of this inverter is to mitigate the CM current by reducing the output harmonic distortions.

II. PROPOSED APPROACH

A 5L-NPC inverter with the best possible number of low voltage switches is used to have high-quality output voltage and to eliminate the leakage current and to reduce output harmonic content for a single-phase grid-tied PV system. The ripple issue of DC-link capacitor voltages and unbalancing in such an application is solved by applying a modulation strategy that can create the required output voltage and add an ability for controlling capacitors' voltages regardless these voltages equal or not to a quarter of the DC-link voltage [21]. The neutral of the grid is linked to a common on which the negative and the positive terminals of the DC-link are connected via parasitic capacitors that can eliminate the leakage current. The proposed PV-based transformerless grid-tied topology with its MLI 5L-NPC inverter is shown in Fig. 4, where 18 PV modules are series-connected of Trina Solar TSM-250 type. On 25C^{o} and 1000 W/m2, the PV string can generate 3000W. Two stray capacitors are connected to the negative and positive points of the DC-link of the PV array and to the ground, which is the neutral of the grid. The system topology, from the grid side, filters by a classical LCL formation with a center tap inductor between the neutral and line branch. A typical 14.4 kVrms source models the utility grid and an ideal pole-mounted a 220V center-tapped transformer, and the central neutral wire is grounded by the resistor Rg. This successive architecture of switches and diodes can be extended to further levels unless limited practically. An MLI leg needs 2(M-1) switches devices, 2(M-2) clamping diodes and (M-1) storage capacitors.

To eliminate unwanted harmonics from the output waveform, a 5L-NPC inverter includes capacitors C1, C2, C3, and C4 at the DC-link with a voltage drop of $V_{dc}/4$ each is proposed. Every level of output voltage for the inverter has a corresponding switching-state. The switching-state consequences of the circuit are shown in Table 1.

TABLE 1. Switching-states and corresponding levels of output voltages.

Switching states	Output Voltage	S1	S2	S3	S4	S5	S6	S7	S8
+1	$V_{dc}/2$	1	1	1	1	0	0	0	0
+2	$V_{dc}/4$	0	1	1	1	1	0	0	0
0	0	0	0	1	1	1	1	0	0
-2	$-V_{dc}/4$	0	0	0	1	1	1	1	0
+1	$-V_{dc}/2$	0	0	0	0	1	1	1	1

A. INVERTER OPERATION

The operation of the developed 5L-NPC inverter can be divided into four regions of switching operation and can be represented by (5-1) switching regions, as demonstrated in Fig. 5. During the region R_1, the switches S_1 and S_5 operate

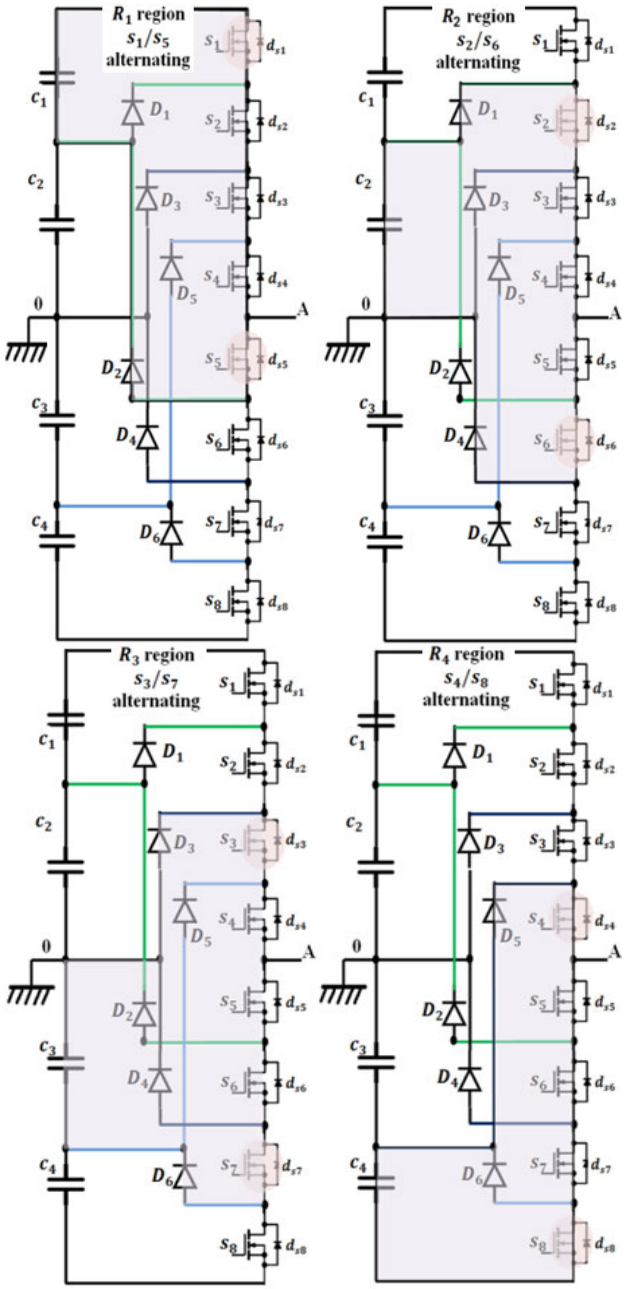

FIGURE 5. Four switching regions for the proposed inverter topology.

alternately to connect the output of the inverter to $V_{dc}/2$ and $V_{dc}/4$ respectively, while S_2, S_3, and S_4 are continue ON. Similarly, during R_2, the switches S_2 and S_6 operate alternately to connect the output of the inverter to $V_{dc}/4$ and 0 respectively, while S_3, S_4, and S_5 are continue ON. For R_3, the switches S_3 and S_7 operate alternately to connect the inverter output to 0 and $-V_{dc}/2$ respectively, while S_4, S_5, and S_6 are continue ON. Finally, during R_4, the switches S_4 and S_8 are working alternately to connect the output of the inverter to $-V_{dc}/4$ and $-V_{dc}/2$ respectively, while S_5, S_6, and S_7 are always ON. The switching regions operate as a two-level inverter but with different forward and freewheeling paths, where M-1 devices contribute to perform that rather than only one. For example; in R_2, the freewheeling path of the upper part includes S_5, and D_2 that connect the inverter output by $V_{dc}/4$ level for the current flow of either negative or positive, while the forward path includes the devices S_2, S_3, S_4, and D_1. Meanwhile, for the down part, the freewheeling current includes S_3, S_4 and D_3 that connects the inverter output to zero levels for either negative or positive flow, while the forward path includes S_3, S_4, and D_4.

A current controller by a Proportional Integral (PI) function is an important part of such an inverter, where a phase-locked loop (PLL) with a simple scheme of current regulator, and a DC-link voltage regulator is used in this work, as depicted in Fig. 6.

P&O technique is employed in an MPPT controller. The function of MPPT is to control the DC voltage regulator automatically by controlling v_{dc_ref} of the inverter to get the DC level of voltage on which the system extracts maximum power from the PV array. The DC voltage regulator determines the necessary reference current i_{d_ref} for the current controller. The current controller uses i_{d_ref}, i_d and the reactive current i_q to determine the necessary reference voltage to the inverter.

The voltage rate of change across the DC capacitors can be written as:

$$\frac{dv_{c_k}}{dt} = \frac{i_{c_k}}{c_k}(S_k - S_{k+4}) \tag{8}$$

where the index $k \in 1, 4\}$, S_k and S_{k+4} are (0) for OFF state and (1) for ON switch state. For single-phase grid-tied applications, the input power may contain second harmonic ripples, and therefore, the voltages of DC-link capacitors will also have this harmonic ripple, and their voltages will not be identical. In this topology, the identical condition is satisfied when $(v_{c_1} = v_{c_2} = v_{c_3} = v_{c_4} = V_{dc}/4)$. In this work, the averaging technique concept is adopted to maintain the balancing of capacitors voltages.

d_{init} is the initial value for v_{dc_ref}.
d_{max} is the upper limit for v_{dc_ref}.
d_{min} is the lower limit for v_{dc_ref}.
Δd is the increment value used to increase/decrease v_{dc_ref}.

B. SWITCHING LOSSES

The switching losses of IGBTs can be calculated as follows:

First-order voltage-drop of IGBT and diode can be given respectively by:

$$V_{CE} = V_t + i\,(t)\,.R_{CE} \tag{9}$$

$$V_{AK} = V_f + i\,(t)\,.R_d \tag{10}$$

where V_{CE}, V_t, V_{AK}, and V_f denote the IGBT collector-emitter at load, IGBT at no load, the diode anode-cathode, and the diode at no-load voltage drops, respectively. R_{CE} and R_d denote the IGBT and the diode ON-state resistance respectively. $i\,(t)$ denotes the current that is given by:

$$i\,(t) = i_o \sin(wt) \tag{11}$$

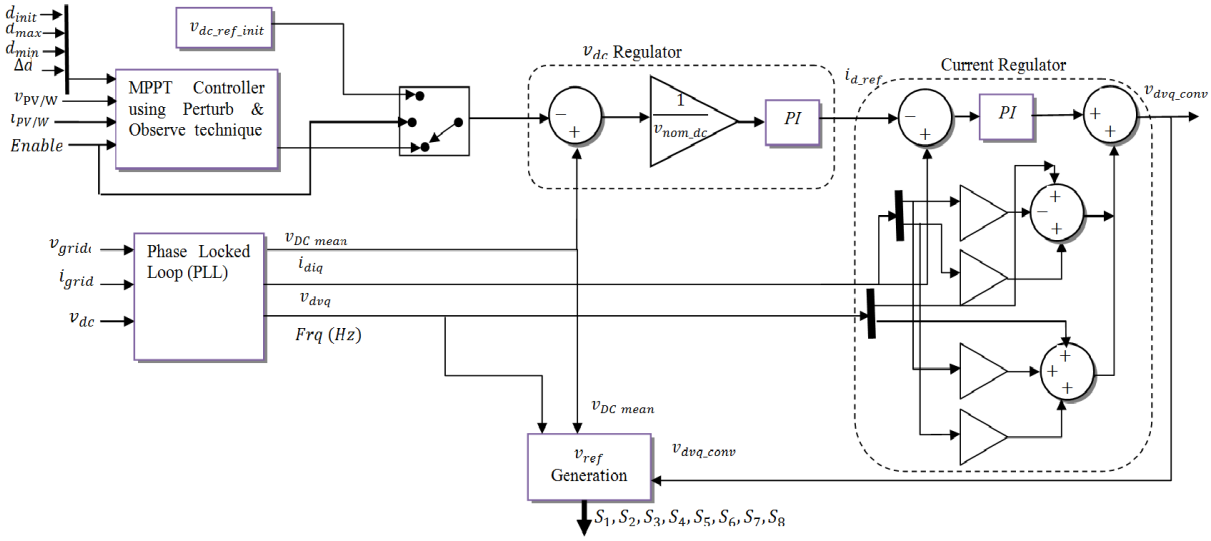

FIGURE 6. Inverter controller diagram of the proposed system.

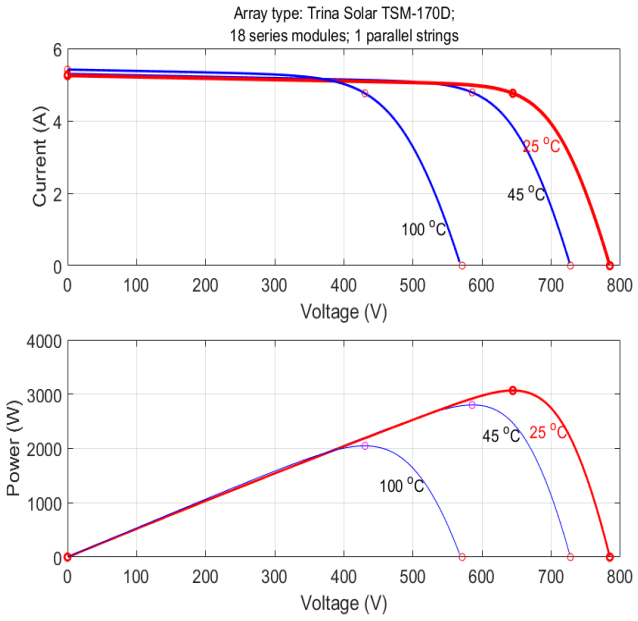

FIGURE 7. The characteristics of a solar PV array that considered in this work.

where i_o denotes the amplitude of the output current. By following the procedure mentioned in [42], [43], the power losses at ON-states and Off-state for the IGBT and diode are given respectively by:

$$P_{onIGBT} = \frac{i_o V_t}{2} + \frac{2mi_o^2 R_{CE}}{3\pi} \quad (12)$$

$$P_{onDiode} = \frac{i_o V_f}{2} + \frac{2m.i_o^2 R_d}{3\pi} \quad (13)$$

$$P_{offIGBT} = \frac{i_o V_t}{\pi} - \frac{i_o V_t m}{2} + \frac{i_o^2 R_{CE}}{4} - \frac{2mi_o^2 R_{CE}}{3\pi} \quad (14)$$

$$P_{offDiode} = \frac{i_o V_f}{\pi} - \frac{i_o V_f m}{2} + \frac{i_o^2 R_d}{4} - \frac{2m.i_o^2 R_d}{3\pi} \quad (15)$$

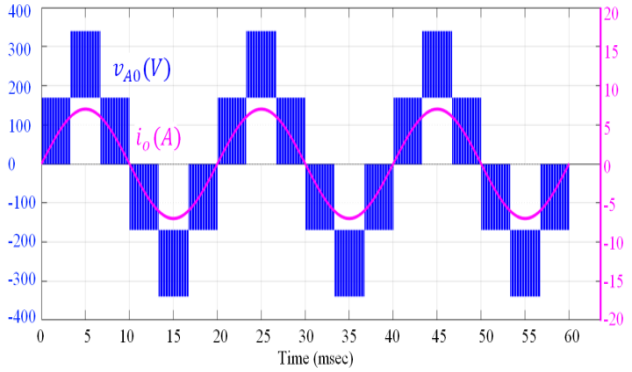

FIGURE 8. Inverter output voltage ($v_{A0} = v_{inv}$) and current (i_o).

Hence, the overall conduction losses can be calculated by:

$$P_{losses} = 4\frac{i_o V_t}{\pi} + m.i_o^2 R_{CE} \quad (16)$$

Accordingly, and based on the data-sheet of the used IGBT, the switching losses for the eight switches for this topology are in the range (3.16-4.2)W, while the conduction losses are in the range (2.12-2.432)W.

III. SIMULATION RESULTS

A grid-tied MLI inverter needs to handle both reactive and active power based on standards such as EN 50438, where an inverter needs to operate at power factor (PF) in the range (0.95 lag - 0.95 lead) [44]. MATLAB has been employed to verify the theoretical concept. The simulation parameters are listed in TABLE 2, while the IV and PV characteristics of the solar PV array is in Fig. 7.

According to the above characteristics for the employed solar PV array, the results of the output voltage and current are shown in Fig. 8, while the simulation results with different values of PF are shown in Fig. 9. An AC value was assigned

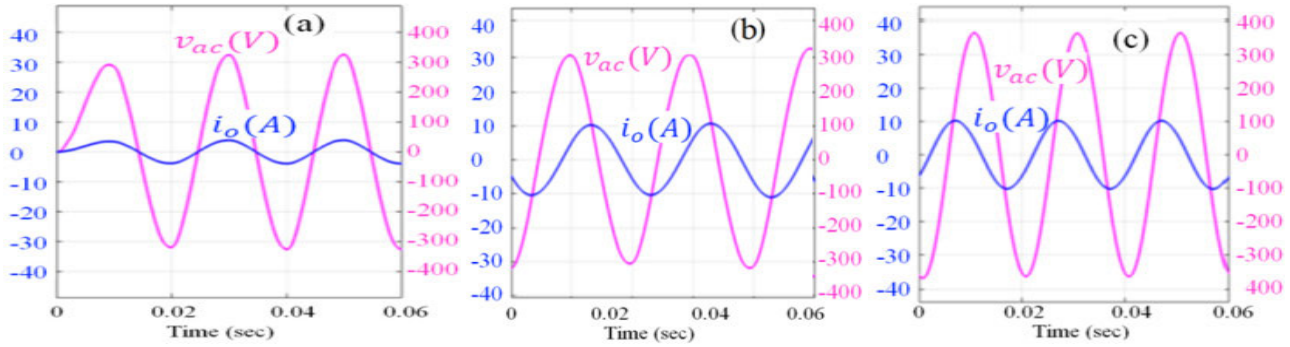

FIGURE 9. Grid-tied hybrid system running under three PF modes; unity (a), lagging (b) and leading (c).

TABLE 2. The list of the parameters in the simulation and prototype.

Parameter explanation	The value
DC Input	630 V
AC Output voltage (v_0)	220 V
Power Nominal	3 kW
Switching Frequency (Fc)	8.5 kHz
Fundamental Frequency (F)	50 Hz
Capacitance (C1, C2, C3, C4)	0.51 μF
Parasitic Capacitance (Cf)	0.47μF
Output filter (Lf)	2 mH
IGBT switches (s1…s8)	IRG4PC40D
Diodes (D1…D6)	STTH3006A

as a reference to operate the proposed system under unity PF (a), lagging PF (b), and leading PF (c). This outcome highlights the high dynamic performance in different modes of PF variation.

It can observe that the grid voltage and current achieve a pure sinusoidal and unity PF on resistive load. Fig. 9 (b) and (c) show that the system dynamic response changes when it is subject to inductive and capacitive part in series with the resistive load, which means that the proposed system has a good dynamic response to the phase angle variation of the reference current from 0° to 43.3°. The Total Harmonic Distortion (THD) of the simulation for the current output is around 1.29% under normal conditions with a DC output current of less than 1 %, which indicates a good performance exhibited for the presented system according to the standard IEC 61727:2004. The simulation measurement of the leakage current for the proposed grid-tied system was around 0 mA, as shown in Fig. 10 (left), which is compared with the case that the PV linked to the ground without stray capacitors, as shown in Fig. 10 (right).

From the above, we can conclude that the proposed system can successfully inject real power to the utility grid at low THD on the output with zero leakage current. A Fast Fourier Transform (FFT) is also used to analyze the output current in a frequency domain, where the fundamental frequency of the output current (50Hz) is 6.23 with THD=1.29%. Therefore, the proposed topology has good CM characteristics.

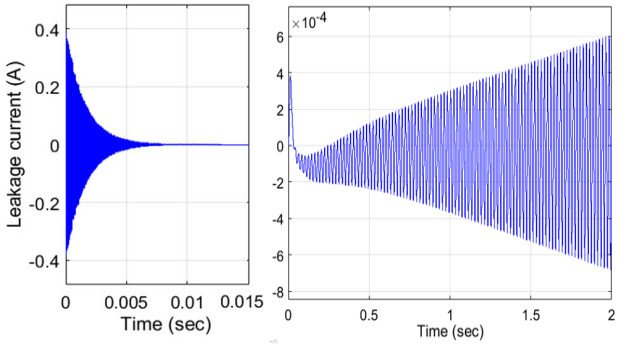

FIGURE 10. Both sources linked to; the stray capacitors (proposed topology) (left), and to ground without stray capacitors (right).

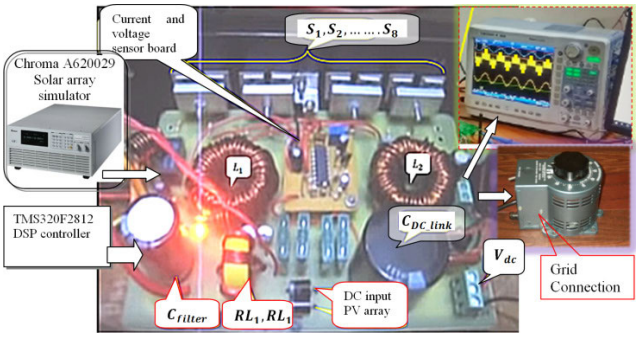

FIGURE 11. A prototype picture for the proposed inverter.

IV. EXPERIMENTAL RESULTS

An experimental prototype is implemented with a 1.1 kW power injection to validate the operation of the proposed system, where measurements have been conducted with the system parameters shown in TABLE 2. The system implements its control algorithm by a development board called the TMS320F2812 DSP controller to create the PWM pulses for the IGBT switches. A picture for the proposed inverter prototype is shown in Fig. 11.

To verify the proposed system experimentally, the system was injected by 1100W real power and 500VAR reactive power. Figure 12(a) shows the PWM control signals for the

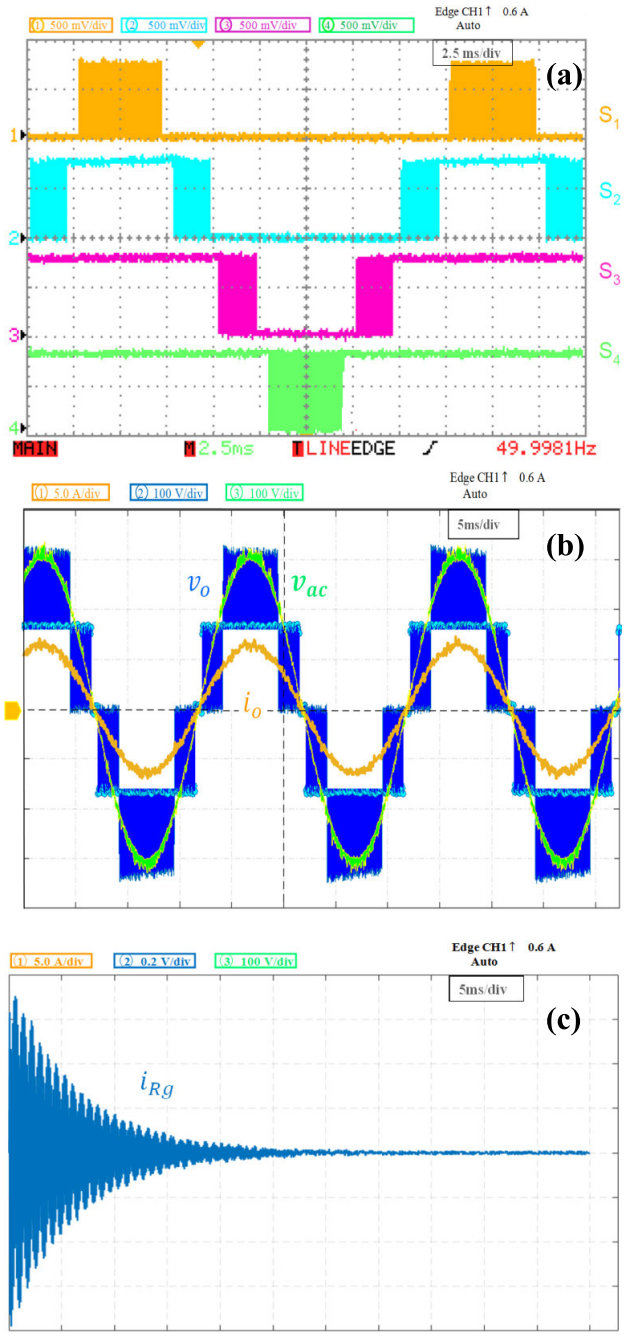

FIGURE 12. Experimental results; (a) PWM control signals for the switches (S1, S2…S4) respectively, (b) with a unity PF, the AC output voltage (v_{ac}) was with (100 V/div), the current was with (5 A/div), and the PWM voltage (v_0) (100 V/div), where the scale of time was (5 ms/div), (c) the leakage current (i_{Rg}) with (0.2 A/div), and the time scale was on (5 ms/div).

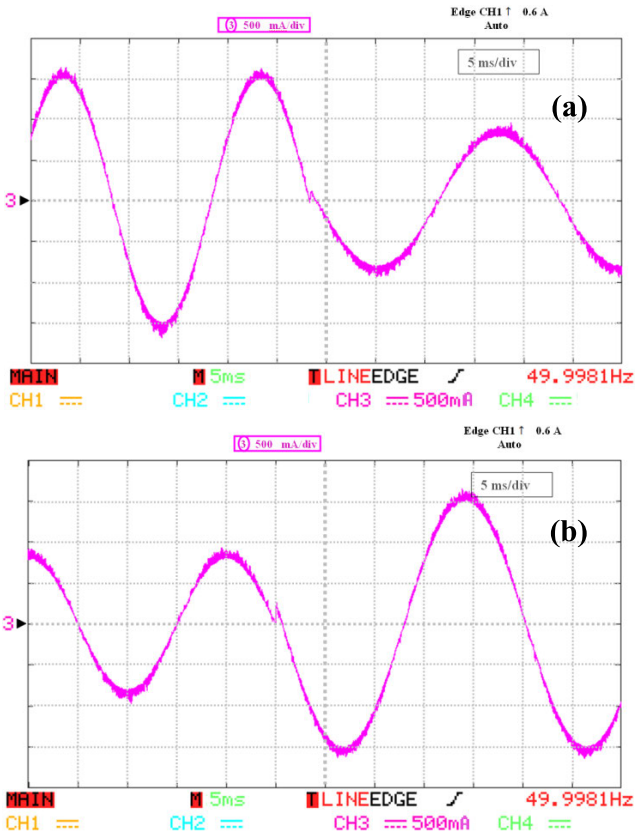

FIGURE 13. Transient response of the output current (i_0) when a step load change (a) from high-low, and (b) back from low to high current (X-axis is 5 ms/div, Y-axis is 500 mA/div).

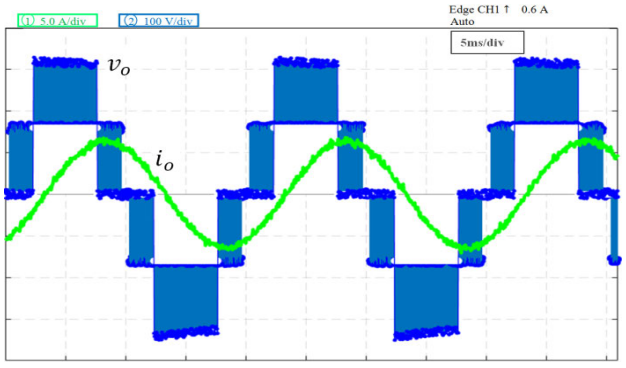

FIGURE 14. Experimental result for lagging power factor condition: the current was with (5 A/div), and the PWM voltage (v_0) (100 V/div), where the scale of time was (5 ms/div).

switches (S1, S2…S4), respectively, which can describe the clamping and operation of the proposed 5L-NPC inverter. For the real power injection, the result shows that the output voltage is in phase with the output current as predicted (see Fig. 12(b)).

It is found that the measured RMS value of leakage current flowing through the inverter was 6.7 mA after few milliseconds, which is under the requirement of the German standard [45], which states that when the leakage current goes over 300 mA, the PV system is required to be disconnected within 0.3 sec. The measured leakage current is shown in Fig. 12(c).

To show the effectiveness of the proposed system under dynamic operating conditions, the transient response of the output current (i_o) during a step change (high-low) of load current is shown in Fig. 13(a), and from (low-high)

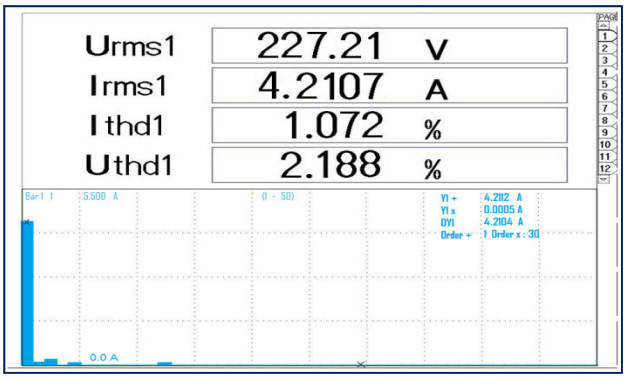

FIGURE 15. THD of output current and voltage.

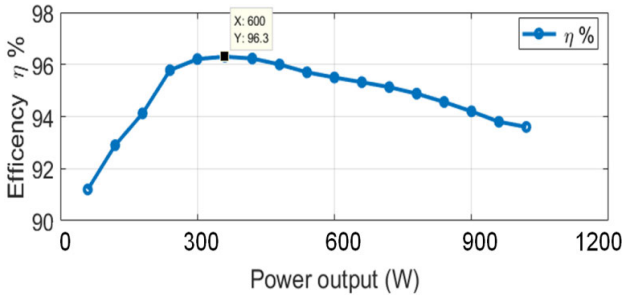

FIGURE 16. Efficiency vs. load power for the proposed inverter.

TABLE 3. A comparison with other single-phase five-level transformerless PV inverters.

Source Topology	S	N-DC	S-losses	CM-V	I_{Rg}	THD
Proposed 5L-NPC	8	1	(3.16-4.2)W	$\frac{V_{dc}}{2}$ to $-\frac{V_{dc}}{2}$	≈ 0	1.07%
[19] Asymmetrical T-type (5L-T-AHB)	6	2	(3.4-6.2)W	$\frac{V_{dc}}{2}$ to $-\frac{V_{dc}}{2}$	2A impulses 50Hz	Not measured
[21] FC- based ANPC	8	1	Not given	$\frac{V_{dc}}{2}$ to $-\frac{V_{dc}}{2}$	Not measured	2.1%
[20] ANPC	12	1	Not given	$\frac{V_{dc}}{2}$ to $-\frac{V_{dc}}{2}$	Not measured	6.89%
[10] 6-H-bridges and 4-SPWM	8	2	Not given	$\frac{V_{dc}}{2}$ to $-\frac{V_{dc}}{2}$	Not measured	1.34%
[47] 5L-ANPC	12	2	Not given	$\frac{V_{dc}}{2}$ to $-\frac{V_{dc}}{2}$	Not measured	Not measured
[48] Switching state sequences for Hybrid type	8	1	Not given	$\frac{V_{dc}}{2}$ to $-\frac{V_{dc}}{2}$	Not measured	19.19%
[42] Modular type half-bridge	6	1	Not given	V_{dc} to $-V_{dc}$	≈ 0	5%

in Fig. 13(b). This result shows that, i_o maintains a sinusoidal waveform with a very low ripple influenced by the switching frequencies.

Fig. 14 shows the waveform of both v_o and i_o under inductive power generation. It is found that the leakage current of the proposed system for both load conditions is approximately 0 mA. It can be seen that on injecting reactive power, no more distortion arises in the grid current. Moreover, Fig. 15 shows the THD measured of the grid current for inductive-power generation, which is 1.07%. Therefore, the system performance is working within IEEE Std. 1547.1TM-2005 requirements [46]. A power analyzer, Fluke 435, has been used to measure the inverter circuit efficiency along with its load power, where the highest efficiency achieved is 96.3 %, as shown in Fig 16.

Table 3 compares the proposed system with other single-phase five-level transformerless PV inverters in several key features. The columns of the table list the topology, number of switches that used to design the inverter (S), number of DC input voltage (N-DC), switching power losses (S-losses), CM voltage (CM-V), leakage current ($\boldsymbol{I_{Rg}}$), and THD.

V. CONCLUSION

A new high-performance transformerless 5L-NPC inverter with its control strategy for a grid-tied PV system has been presented. The major advantages of the presented system can be brief as follows:

1. The topology of employing diode clamping MLI with suitable stray capacitors makes the leakage current to flow through the system in a very low value reaches zero. Furthermore, the system offers a connection between the DC-link pass bar of a solar PV array with the grid neutral terminal that results in zero leakage current.
2. The operation of the employed five-level topology results in high performance for the harmonic distortion that allows the reduction of filter components as compared with lower MLIs.
3. The proposed 5L-NPC topology eliminated the CM leakage current with 1.07% THD by using eight power switches.

The results confirmed the above-stated advantages, and the proposed system offers approximately similar characteristics in reactive and real power injections. Therefore, the proposed inverter topology and its modulation scheme were a suitable and attractive solution for single-phase grid-tied PV systems. Although the proposed 5L-NPC system achieved zero CM leakage current with a very-low THD, the design is limited by eight switches that are recommended to be reduced in future work. Moreover, the presented system solved the balancing issue of the DC-link capacitors' voltages that required for proper operation by a modulation strategy inspired in [21], we recommend easier algorithms to solve such issue.

REFERENCES

[1] S. Padmanaban, N. Priyadarshi, J. B. Holm-Nielsen, M. S. Bhaskar, F. Azam, A. K. Sharma, and E. Hossain, "A novel modified sine–cosine optimized MPPT algorithm for grid integrated PV system under real operating conditions," *IEEE Access*, vol. 7, pp. 10467–10477, 2019.

[2] N. Priyadarshi, S. Padmanaban, M. S. Bhaskar, F. Blaabjerg, and A. Sharma, "Fuzzy SVPWM-based inverter control realisation of grid integrated photovoltaic-wind system with fuzzy particle swarm optimisation maximum power point tracking algorithm for a grid-connected PV/wind power generation system: Hardware implementation," *IET Electr. Power Appl.*, vol. 12, no. 7, pp. 962–971, Aug. 2018.

[3] N. Priyadarshi, S. Padmanaban, P. Kiran Maroti, and A. Sharma, "An extensive practical investigation of FPSO–based MPPT for grid integrated PV system under variable operating conditions with anti–islanding protection," *IEEE Syst. J.*, vol. 13, no. 2, pp. 1861–1871, Jun. 2019.

[4] N. Priyadarshi, S. Padmanaban, J. B. Holm-Nielsen, F. Blaabjerg, and M. S. Bhaskar, "An experimental estimation of hybrid ANFIS–PSO-based MPPT for PV grid integration under fluctuating sun irradiance," *IEEE Syst. J.*, to be published.

[5] N. Priyadarshi, S. Padmanaban, S. Member, M. S. Bhaskar, and F. Blaabjerg, "A hybrid photovoltaic-fuel cell-based single-stage grid integration with Lyapunov control scheme," *IEEE Syst. J.*, to be published.

[6] S. Padmanaban, N. Priyadarshi, M. S. Bhaskar, J. B. Holm-Nielsen, E. Hossain, and F. Azam, "A hybrid photovoltaic–fuel cell for grid integration with jaya–based maximum power point tracking: Experimental performance evaluation," *IEEE Access*, vol. 7, pp. 82978–82990, 2019.

[7] B. K. Bose, "Global energy scenario and impact of power electronics in 21st century," *IEEE Trans. Ind. Electron.*, vol. 60, no. 7, pp. 2638–2651, Jul. 2013.

[8] J. Myrzik, "Novel inverter topologies for single-phase stand-alone or grid-connected photovoltaic systems," in *Proc. Int. Conf. Power Electron. Drive Syst.*, Aug. 2001.

[9] S. Kjaer, J. Pedersen, and F. Blaabjerg, "A review of single–phase grid–connected inverters for photovoltaic modules," *IEEE Trans. Ind. Appl.*, vol. 41, no. 5, pp. 1292–1306, Sep. 2005.

[10] I. Colak, E. Kabalci, and R. Bayindir, "Review of multilevel voltage source inverter topologies and control schemes," *Energy Convers. Manage.*, vol. 52, no. 2, pp. 1114–1128, Feb. 2011.

[11] H. Abu-Rub, J. Holtz, J. Rodriguez, and G. Baoming, "Medium-voltage multilevel converters–state of the art, challenges, and requirements in industrial applications," *IEEE Trans. Ind. Electron.*, vol. 57, no. 8, pp. 2581–2596, Aug. 2010.

[12] K. K. Gupta and S. Jain, "A novel multilevel inverter based on switched DC sources," *IEEE Trans. Ind. Electron.*, vol. 61, no. 7, pp. 3269–3278, Jul. 2014.

[13] L. Franquelo, J. Rodriguez, J. Leon, S. Kouro, R. Portillo, and M. Prats, "The age of multilevel converters arrives," *IEEE Ind. Electron. Mag.*, vol. 2, no. 2, pp. 28–39, Jun. 2008.

[14] R. Gonzalez, E. Gubia, J. Lopez, and L. Marroyo, "Transformerless single–phase multilevel–based photovoltaic inverter," *IEEE Trans. Ind. Electron.*, vol. 55, no. 7, pp. 2694–2702, Jul. 2008.

[15] Ó. López, F. D. Freijedo, A. G. Yepes, P. Fernández-Comesaña, J. Malvar, R. Teodorescu, and J. Doval-Gandoy, "Eliminating ground current in a transformerless photovoltaic application," *IEEE Trans. Energy Convers.*, vol. 25, no. 1, pp. 140–147, Mar. 2010.

[16] H. Xiao and S. Xie, "Leakage current analytical model and application in single–phase transformerless photovoltaic grid–connected inverter," *IEEE Trans. Electromagn. Compat.*, vol. 52, no. 4, pp. 902–913, Nov. 2010.

[17] M. C. Cavalcanti, A. M. Farias, K. C. Oliveira, F. A. S. Neves, and J. L. Afonso, "Eliminating leakage currents in neutral point clamped inverters for photovoltaic systems," *IEEE Trans. Ind. Electron.*, vol. 59, no. 1, pp. 435–443, Jan. 2012.

[18] K. C. Oliveira, M. C. Cavalcanti, J. L. Afonso, A. M. Farias, and F. A. S. Neves, "Transformerless photovoltaic systems using neutral point clamped multilevel inverters," in *Proc. IEEE Int. Symp. Ind. Electron.*, Jul. 2010.

[19] G. E. Valderrama, G. V. Guzman, E. I. Pool-Mazun, P. R. Martinez-Rodriguez, M. J. Lopez-Sanchez, and J. M. S. Zuniga, "A single–phase asymmetrical T–type five–level transformerless PV inverter," *IEEE J. Emerg. Sel. Topics Power Electron.*, vol. 6, no. 1, pp. 140–150, Mar. 2018.

[20] K. Wang, Z. Zheng, Y. Li, K. Liu, and J. Shang, "Neutral–point potential balancing of a five–level active neutral–point-clamped inverter," *IEEE Trans. Ind. Electron.*, vol. 60, no. 5, pp. 1907–1918, May 2013.

[21] H. R. Teymour, D. Sutanto, K. M. Muttaqi, and P. Ciufo, "A novel modulation technique and a new balancing control strategy for a single–phase five–level ANPC converter," *IEEE Trans. Ind. Appl.*, vol. 51, no. 2, pp. 1215–1227, Mar. 2015.

[22] S. B. Kjær, "Design and control of an inverter for photovoltaic applications," Dept. Energy Technol., Univ. Aalborg, Aalborg, Denmark, 2005.

[23] M. Islam, S. Mekhilef, and M. Hasan, "Single phase transformerless inverter topologies for grid-tied photovoltaic system: A review," *Renew. Sustain. Energy Rev.*, vol. 45, pp. 69–86, May 2015.

[24] O. Lopez, R. Teodorescu, F. Freijedo, and J. Dovalgandoy, "Leakage current evaluation of a singlephase transformerless PV inverter connected to the grid," in *Proc. Conf. IEEE Appl. Power Electron. Conf. Expo. (APEC)*, Feb. 2007.

[25] B. Gu, J. Dominic, J.-S. Lai, C.-L. Chen, T. Labella, and B. Chen, "High reliability and efficiency single–phase transformerless inverter for grid–connected photovoltaic systems," *IEEE Trans. Power Electron.*, vol. 28, no. 5, pp. 2235–2245, May 2013.

[26] G. Rizzoli, M. Mengoni, L. Zarri, A. Tani, G. Serra, and D. Casadei, "Comparison of single-phase H4, H5, H6 inverters for transformerless photovoltaic applications," in *Proc. IECON Ind. Electron. Conf.*, Oct. 2016.

[27] M. Victor, F. Greizer, S. Bremicker, and U. Hübler, "Method of converting a direct current voltage from a source of direct current voltage, more specifically from a photovoltaic source of direct current voltage, into a alternating current voltage," U.S. Patent 7 411 802 B2, Aug. 12, 2008.

[28] T. Dragicevic, J. Vasquez, J. Guerrero, and D. Škrlec, "Advanced LVDC electrical power architectures and microgrids: A step toward a new generation of power distribution networks," *IEEE Electrific. Mag.*, vol. 2, no. 1, pp. 54–65, Mar. 2014.

[29] R. Gonzalez, J. Coloma, L. Marroyo, J. Lopez, and P. Sanchis, "Single-phase inverter circuit for conditioning and converting DC electrical energy into AC electrical energy," Eur. Patent Appl. EP 2 053 730 A1, 2009.

[30] L. Zhang, K. Sun, Y. Xing, and M. Xing, "H6 transformerless full–bridge PV grid–tied inverters," *IEEE Trans. Power Electron.*, vol. 29, no. 3, pp. 1229–1238, Mar. 2014.

[31] W. Yu, J.-S.-J. Lai, H. Qian, and C. Hutchens, "High–efficiency MOSFET inverter with H6-type configuration for photovoltaic nonisolated AC–module applications," *IEEE Trans. Power Electron.*, vol. 26, no. 4, pp. 1253–1260, Apr. 2011.

[32] L. Zhang, K. Sun, L. Feng, H. Wu, and Y. Xing, "A family of neutral point clamped full–bridge topologies for transformerless photovoltaic grid–tied inverters," *IEEE Trans. Power Electron.*, vol. 28, no. 2, pp. 730–739, Feb. 2013.

[33] H. Xiao, S. Xie, Y. Chen, and R. Huang, "An optimized transformerless photovoltaic grid–connected inverter," *IEEE Trans. Ind. Electron.*, vol. 58, no. 5, pp. 1887–1895, May 2011.

[34] N. Vazquez, M. Rosas, C. Hernandez, E. Vazquez, and F. J. Perez-Pinal, "A new common–mode transformerless photovoltaic inverter," *IEEE Trans. Ind. Electron.*, vol. 62, no. 10, pp. 6381–6391, Oct. 2015.

[35] Y. Gu, W. Li, Y. Zhao, B. Yang, C. Li, and X. He, "Transformerless inverter with virtual dc bus concept for cost–effective grid–connected PV power systems," *IEEE Trans. Power Electron.*, vol. 28, no. 2, pp. 793–805, Feb. 2013.

[36] J. F. Ardashir, M. Sabahi, S. H. Hosseini, F. Blaabjerg, E. Babaei, and G. B. Gharehpetian, "A single–phase transformerless inverter with charge pump circuit concept for grid–tied PV applications," *IEEE Trans. Ind. Electron.*, vol. 64, no. 7, pp. 5403–5415, Jul. 2017.

[37] A. Anurag, N. Deshmukh, A. Maguluri, and S. Anand, "Integrated DC–DC converter based grid–connected transformerless photovoltaic inverter with extended input voltage range," *IEEE Trans. Power Electron.*, vol. 33, no. 10, pp. 8322–8330, Oct. 2018.

[38] J.-M. Shen, H.-L. Jou, and J.-C. Wu, "Novel transformerless grid–connected power converter with negative grounding for photovoltaic generation system," *IEEE Trans. Power Electron.*, vol. 27, no. 4, pp. 1818–1829, Apr. 2012.

[39] N. Vazquez, J. Vazquez, J. Vaquero, C. Hernandez, E. Vazquez, and R. Osorio, "Integrating two stages as a common–mode transformerless photovoltaic converter," *IEEE Trans. Ind. Electron.*, vol. 64, no. 9, pp. 7498–7507, Sep. 2017.

[40] W. Li, Y. Gu, H. Luo, W. Cui, X. He, and C. Xia, "Topology review and derivation methodology of single–phase transformerless photovoltaic inverters for leakage current suppression," *IEEE Trans. Ind. Electron.*, vol. 62, no. 7, pp. 4537–4551, Jul. 2015.

[41] Y. P. Siwakoti and F. Blaabjerg, "Common-ground-type transformerless inverters for single–phase solar photovoltaic systems," *IEEE Trans. Ind. Electron.*, vol. 65, no. 3, pp. 2100–2111, Mar. 2018.

[42] A. Kadam and A. Shukla, "A multilevel transformerless inverter employing ground connection between PV negative terminal and grid neutral point," *IEEE Trans. Ind. Electron.*, vol. 64, no. 11, pp. 8897–8907, Nov. 2017.

[43] A. I. Maswood, "A switching loss study in SPWM IGBT inverter," in *Proc. IEEE 2nd Int. Power Energy Conf. (PECon)*, vol. 8, Dec. 2008, pp. 609–613.

[44] B.-I. Craciun, T. Kerekes, D. Sera, and R. Teodorescu, "Overview of recent Grid Codes for PV power integration," in *Proc. Int. Conf. Optim. Elect. Electron. Equip. (OPTIM)*, 2012.

[45] E. Mail and I. Rolle, *DKE Deutsche Kommission Elektrotechnik Elektronik Informationstechnik im DIN und VDE*. Notes, 2009.

[46] *IEEE Standard Conformance Equipment Interconnecting Electric Power Systems*, IEEE Standard 547.1-2005, 2005.

[47] E. Burguete, J. Lopez, and M. Zabaleta, "New five–level active neutral-point-clamped converter," *IEEE Trans. Ind. Appl.*, vol. 51, no. 1, pp. 440–447, Jan. 2015.

[48] M. Ma, X. Song, W. Cao, X. He, and B. Ji, "Optimised phase disposition pulse-width modulation strategy for hybrid-clamped multilevel inverters using switching state sequences," *IET Power Electron.*, vol. 8, no. 7, pp. 1095–1103, Jul. 2015.

[49] H. Sepahvand, J. Liao, M. Ferdowsi, and K. Corzine, "Capacitor voltage regulation in single-DC-source cascaded H–bridge multilevel converters using phase–shift modulation," *IEEE Trans. Ind. Electron.*, vol. 60, no. 9, pp. 3619–3626, May 2013.

[50] Z. Du, B. Ozpineci, L. M. Tolbert, and J. N. Chiasson, "DC-AC cascaded H-bridge multilevel boost inverter with no inductors for electric/hybrid electric vehicle applications," *IEEE Trans. Ind. Appl.*, to be published.

[51] S. Vazquez, J. Leon, L. Franquelo, J. Padilla, and J. Carrasco, "DC-voltage-ratio control strategy for multilevel cascaded converters fed with a single DC source," *IEEE Trans. Ind. Electron.*, vol. 56, no. 7, pp. 2513–2521, Jul. 2009.

[52] B. Xiao, L. Hang, J. Mei, C. Riley, L. M. Tolbert, and B. Ozpineci, "Modular cascaded H–bridge multilevel PV inverter with distributed MPPT for grid–connected applications," *IEEE Trans. Ind. Appl.*, vol. 51, no. 2, pp. 1722–1731, Mar. 2015.

[53] J. Mei, B. Xiao, K. Shen, L. M. Tolbert, and J. Y. Zheng, "Modular multilevel inverter with new modulation method and its application to photovoltaic grid–connected generator," *IEEE Trans. Power Electron.*, vol. 28, no. 11, pp. 5063–5073, Nov. 2013.

[54] D. Tiku, "Modular multilevel MMI(HB) topology for single–stage grid connected PV plant," in *IET Seminar Dig.*, 2015.

[55] M. R. Islam, A. M. Mahfuz-Ur-Rahman, M. M. Islam, Y. G. Guo, and J. G. Zhu, "Modular medium–voltage grid–connected converter with improved switching techniques for solar photovoltaic systems," *IEEE Trans. Ind. Electron.*, vol. 64, no. 11, pp. 8887–8896, Nov. 2017.

[56] A. Nabae, I. Takahashi, and H. Akagi, "A new neutral-point-clamped PWM inverter," *IEEE Trans. Ind. Appl.*, vol. IA-17, no. 5, pp. 518–523, Sep. 1981.

[57] A. Taallah and S. Mekhilef, "Active neutral point clamped converter for equal loss distribution," *IET Power Electron.*, vol. 7, no. 7, pp. 1859–1867, Jul. 2014.

[58] J. Rodriguez, S. Bernet, P. K. Steimer, and I. E. Lizama, "A survey on neutral-point-clamped inverters," *IEEE Trans. Ind. Electron.*, vol. 57, no. 7, pp. 2219–2230, Jul. 2010.

[59] J. Jana, H. Saha, and K. Das Bhattacharya, "A review of inverter topologies for single-phase grid-connected photovoltaic systems," *Renew. Sustain. Energy Rev.*, vol. 72, pp. 1256–1270, May 2017.

[60] M. Islam and S. Mekhilef, "H6-type transformerless single-phase inverter for grid-tied photovoltaic system," *IET Power Electron.*, vol. 8, no. 4, pp. 636–644, Apr. 2015.

[61] M. Islam, N. Afrin, and S. Mekhilef, "Efficient single phase transformerless inverter for grid–tied PVG system with reactive power control," *IEEE Trans. Sustain. Energy*, vol. 7, no. 3, pp. 1205–1215, Jul. 2016.

[62] S. K. Chattopadhyay and C. Chakraborty, "A new asymmetric multilevel inverter topology suitable for solar PV applications with varying irradiance," *IEEE Trans. Sustain. Energy*, vol. 8, no. 4, pp. 1496–1506, Oct. 2017.

[63] L. Wang, Q. H. Wu, and W. Tang, "Novel cascaded switched–diode multilevel inverter for renewable energy integration," *IEEE Trans. Energy Convers.*, vol. 32, no. 4, pp. 1574–1582, Dec. 2017.

[64] E. Babaei and S. H. Hosseini, "New cascaded multilevel inverter topology with minimum number of switches," *Energy Convers. Manage.*, vol. 50, no. 11, pp. 2761–2767, Nov. 2009.

[65] M. Islam and S. Mekhilef, "Efficient transformerless MOSFET inverter for a grid–tied photovoltaic system," *IEEE Trans. Power Electron.*, vol. 31, no. 9, pp. 6305–6316, Sep. 2016.

[66] P. Mehta, A. Kunapara, and N. Karelia, "Improvement in switching strategy used for even loss distribution in ANPC multilevel inverter," *Procedia Technol.*, vol. 21, pp. 386–392, 2015.

[67] P. Lezana and R. Aceiton, "Hybrid multicell converter: Topology and modulation," *IEEE Trans. Ind. Electron.*, vol. 58, no. 9, pp. 3938–3945, Sep. 2011.

[68] V. Dargahi, K. Corzine, G. K. Venayagamoorthy, and A. K. Sadigh, "Hybrid double flying capacitor multicell converter and its application in grid-tied renewable energy resources," *IET Gener., Transmiss. Distrib.*, vol. 9, no. 10, pp. 947–956, Jul. 2015.

[69] S. R. Pulikanti, G. Konstantinou, and V. G. Agelidis, "Hybrid seven–level cascaded active neutral-point-clamped-based multilevel converter under SHE–PWM," *IEEE Trans. Ind. Electron.*, vol. 60, no. 11, pp. 4794–4804, Nov. 2013.

[70] H. Wu, L. Zhu, F. Yang, T. Mu, and H. Ge, "Dual-DC-port asymmetrical multilevel inverters with reduced conversion stages and enhanced conversion efficiency," *IEEE Trans. Ind. Electron.*, vol. 64, no. 3, pp. 2081–2091, Mar. 2017.

[71] C. A. Silva, L. A. Cordova, P. Lezana, and L. Empringham, "Implementation and control of a hybrid multilevel converter with floating dc links for current waveform improvement," *IEEE Trans. Ind. Electron.*, vol. 58, no. 6, pp. 2304–2312, Jun. 2011.

[72] M. Veenstra and A. Rufer, "Control of a hybrid asymmetric multilevel inverter for competitive medium–voltage industrial drives," *IEEE Trans. Ind. Appl.*, vol. 41, no. 2, pp. 655–664, Mar. 2005.

[73] J. Rodriguez, J.-S. Lai, and F. Zheng Peng, "Multilevel inverters: A survey of topologies, controls, and applications," *IEEE Trans. Ind. Electron.*, vol. 49, no. 4, pp. 724–738, Aug. 2002.